The Journal of Experimental Biology 205, 2479–2488 (2002)
Printed in Great Britain © The Company of Biologists Limited 2002
JEB4033

Roughness-dependent friction force of the tarsal claw system in the beetle *Pachnoda marginata* (Coleoptera, Scarabaeidae)

Zhendong Dai[1,2], Stanislav N. Gorb[1,*] and Uli Schwarz[1]

[1]*Biological Microtribology Group, Division II, Max-Planck-Institute of Developmental Biology, Spemannstrasse 35, D-72076, Tuebingen, Germany* and [2]*College of Mechanical and Electric Engineering, Nanjing University of Aeronautics and Astronautics, 29 Yudao Street210016, Nanjing, China*

*Author for correspondence at present address: Evolutionary Biomaterials Group, Max-Planck-Institut fuer Metallforschung, Heisenbergstrasse 3, D-70569 Stuttgart, Germany (e-mail: s.gorb@mf.mpg.de)

Accepted 15 May 2002

Summary

This paper studies slide-resisting forces generated by claws in the free-walking beetle *Pachnoda marginata* (Coleoptera, Scarabaeoidea) with emphasis on the relationship between the dimension of the claw tip and the substrate texture. To evaluate the force range by which the claw can interact with a substrate, forces generated by the freely moving legs were measured using a load cell force transducer. To obtain information about material properties of the claw, its mechanical strength was tested in a fracture experiment, and the internal structure of the fractured claw material was studied by scanning electron microscopy. The bending stress of the claw was evaluated as 143.4–684.2 MPa, depending on the cross-section model selected. Data from these different approaches led us to propose a model explaining the saturation of friction force with increased texture roughness. The forces are determined by the relative size of the surface roughness R_a (or an average particle diameter) and the diameter of the claw tip. When surface roughness is much bigger than the claw tip diameter, the beetle can grasp surface irregularities and generate a high degree of attachment due to mechanical interlocking with substrate texture. When R_a is lower than or comparable to the claw tip diameter, the frictional properties of the contact between claw and substrate particles play a key role in the generation of the friction force.

Key words: friction, locomotion, leg, cuticle, insect, biomaterials, biomechanics, material properties, *Pachnoda marginata*, Scarabaeidae, Coleoptera.

Introduction

Beetles (*Coleoptera*) are the largest group of insects and inhabit nearly every biological niche. During evolution, to enable walking and attachment on the variety of substrata, beetles developed various leg adaptations (Stork, 1987). To generate propulsive forces, a locomotory mechanism must be able to generate sufficient grip or friction with the substrate. Specialized adhesive tarsal setae of representatives of some beetle families provide a mechanism of attachment to plant surfaces, because such natural substrata can be very smooth indeed (Stork, 1983a,b). Claws are structures adapted to diverse rough textures (Nachtigall, 1974). Attachment mechanisms of specialized adhesive devices, such as arolium, pulvilli, euplantulae, tarsal hairs etc., have been studied experimentally in a variety of insect taxa such as flies (Bauchhenss, 1979; Walker et al., 1985; Gorb, 1998), bugs (Gillett and Wigglesworth, 1932), ants (Federle et al., 2000), orthopterans (Gorb et al., 2000; Jiao et al., 2000), and beetles (Stork, 1980; Ishii, 1987; Eisner and Aneshansley, 2000).

The mechanism of claw action on rough textures in various animals seems at first glance to be trivial (Cartmill, 1985). However, it is still not clear what substrate roughness is critical for this attachment system, and how attachment force is related to claw dimension and substrate texture. It is known that friction forces, generated by claws, are part of the autonomous action of the bee pretarsus. During the tarsus placement on the substrate, claws contact with the surface. If the grip is sufficient to prevent sliding, claws become the driving mechanism for generation of propulsive forces. If the claws slide along the substrate, arolium, which is responsible for attachment on smooth substrata, will be mechanically activated (Snodgrass, 1956; Federle et al., 2001). The insect unguitactor apparatus, which is connected to the claws on one side and to the tendon of the claw flexor muscle on the other side, plays an important role in claw kinematics (Heinzeller et al., 1989; Seifert and Heinzeller, 1989; Radnikow and Bässler, 1991). It has been hypothesized that claws, interlocked with the surface, cause interlocking of the unguitractor plate when the claw flexor muscle is contracted (Gorb, 1996). This mechanism allows stable claw holding in a bent position for a long time with a minimum of muscular force expenditure.

This paper studies the attachment forces generated by claws in the free-walking beetle with an emphasis on the relationship

between the dimension of the claw tip and the substrate texture. *Pachnoda marginata* (Coleoptera, Scarabaeidae) was selected for experiments because this species does not possess any specialized attachment devices for smooth substrata. To evaluate the force range by which the claw can interact with substrate, forces generated by the freely moving legs were measured using the load cell force transducer. To obtain information about material properties of the claw, its mechanical strength was tested in a fracture experiment, and the internal structure of the claw material was studied by scanning electron microscopy. Data obtained by these different approaches led us to propose a model explaining saturation of attachment force with an increased texture roughness.

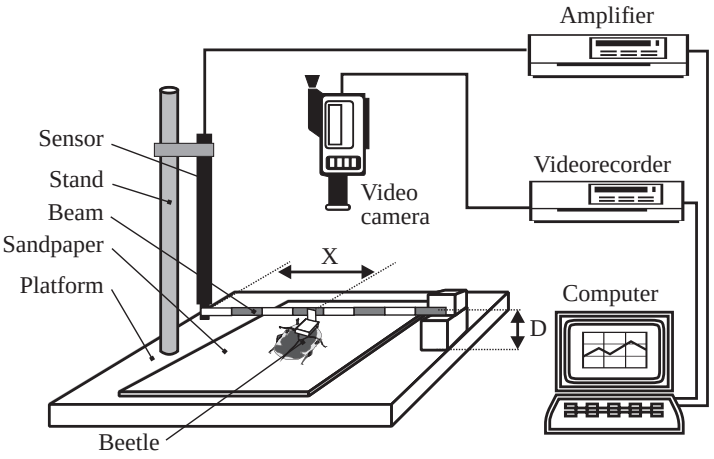

Fig. 1. Force measurement system of the beetle *Pachnoda marginata*. The system consists of a platform covered by sandpaper, force sensor, and videorecorder. 100 mm long crossbeam was connected to the force sensor on one side and supported on the other side. The height of the beam (D) relative to the sandpaper plane was adjusted to be 1–3 mm higher than the dorsal surface of the walking beetle. The force generated by the beetle was transferred by the beam to the sensor and monitored by the load cell force transducer and the signal amplified by the MP-100 system (Biopac system Inc. USA). The data were finally sampled and processed with the aid of a computer. A binocular microscope equipped with a video camera connected to a videorecorder was used to collect images of the beetle during the force measurements. From these images, the distance from the beetle to the sensor (X) was obtained. Force generated by the beetle F_B was calculated as $F_B=100F_S/(100–X)$, where F_S is the force measured with the sensor.

Materials and methods

Animals and surfaces used in experiments

Beetles (*Pachnoda marginata* Drury, Scarabaeoidea) were obtained in the larval stage from a supplier. After pupation and hatching, adults were kept under normal room conditions (20–24 °C). Beetles were individually weighed prior to the experiments (mass=1.002±0.233 g, mean ± S.D., N=9). Intact and broken claws were air-dried for 4 weeks, sputter-coated with gold–palladium (10 nm) and examined in a Hitachi S-800 scanning electron microscope (SEM) at 20 kV. A SEM study of the claw material was also carried out with a freshly fixed, dehydrated and critical-point-dried claw. There was no significant difference in the structure of this stiff material from claws that had been air-dried or critical-point-dried.

The sandpaper used for the experiments is covered by Al_2O_3 particles (Wirtz-Buehler GmbH, Düsseldorf, Germany). The grit number, particle diameter and surface roughness (R_a) are listed in Table 1. Surface profile was measured using the perthometer M1 (Mahr GmbH, Göttingen, Germany). R_a was defined as the square root value of the difference between heights to its average height (see Appendix A). R_a was not measured for the sandpaper types P60 and P100, because their roughness was beyond the measuring range of the perthometer.

Force measurements of beetles walking on different textures

To measure forces generated by walking beetles on different textures, a force sensor (load cell force transducer, 10 g) was used (Biopac System Inc. USA), mounted on a stand connected to the platform (Fig. 1). A metallic cross beam was used to transmit the beetle force to the sensor. One side of the crossbeam was connected to the sensor and another supported by the platform. The height of the beam was adjustable in a vertical direction. The distance between the beam and the sandpaper surface was adjusted to a suitable height (D) corresponding to the beetle's height (5–7 mm) plus 1–3 mm. The force sensor was attached to an amplifier and computer-based data-acquisition and processing system. The beetle's position was monitored by a video camera mounted on a binocular microscope. Experiments were video-recorded, and geometrical parameters were obtained from single video-frames.

The platform was covered by sandpaper of different particle size (Table 1). A beetle with a Plexiglas angle, glued onto the

Table 1. *Variables of the sandpaper used in experiments*

	Type of sandpaper					
Variables	P60†	P120†	P280*	P400*	P0*	12 μm†
Mean diameter (μm)	269	125	52.2±2.0	35.0±1.5	18.3±1.0	12
Roughness R_a (μm)	–	–	8.464	7.999	5.996	2.408
***F*/W** from experiments	38	22	26	19	3	0.9

Values are means ± S.D. *N=10; †roughness data obtained from supplier.
***F*/W**, force ratio (see Fig. 7).

dorsal surface of its thorax, walked on the sandpaper in the direction of the crossbeam until the angle contacted with the beam. Since the angle was only about 3% of the beetle's weight, it did not change the beetle's locomotion. The beetle continued to walk in the same direction for a while trying to overcome the obstacle by pressing against the crossbeam. Forces generated by such an action were monitored by the sensor. Knowing the distance (30–40 mm) between the contact point of the Plexiglas angle and the crossbeam (X), the force monitored by the sensor F_S was recalculated in the actual force generated by the beetle F_B:

$$F_B = \frac{100}{100 - X} F_S . \quad (1)$$

The forces we measured were the forces generated when a beetle encounters an obstacle. However, this fact does not change the character of the relationship between claws and substrate. Moreover, the beetle's landscape normally consists of obstacles.

The sensor was calibrated at the point where the crossbeam was connected before and after an experiment (sensitivity 10 μN). 3–5 beetles with three repetitions per individual were used for the experiment with each sandpaper.

Forces of the freely moving legs

To evaluate forces generated by a freely moving single leg, the beetle was fixed to a micromanipulator (World Precision Instruments Inc.), enabling adjustment of the beetle position relative to the sensor. Whenever the beetle grasped and pulled the sensor tip, the force was monitored and recorded. Five repetitions each for the forelegs, midlegs and hindlegs were done in three individual beetles.

Mechanical strength of the claw

The mechanical properties of the claw were tested on a Biotester Basalt-01 (Tetra GmbH, Ilmenau, Germany) (for details, see Gorb et al., 2000). The claw of a freshly killed beetle was glued with cyanacrylat glue (5925 Universal, S. Kisling & Cie AG; Zürich, Switzerland) to the platform. The metal spring was moved downwards, pressing with its tip against the claw tip until the claw was broken (Fig. 4A). The deflection of the spring tip was monitored by the fiber-optical sensor. Knowing the spring constant, the deflection was recalculated in the force. The maximum force of force–distance curves was used for calculations of braking stress. Since claw geometry of the fore-, mid- and hindlegs is constant (Fig. 2A), seven claws from different legs were tested.

Results

Claw structure

While walking on a sandpaper surface, the beetle contacts the surface with its claw tips and, depending on the friction force in the contact area, generates propulsive movements. Fore- and midlegs pull themselves posteriorly or

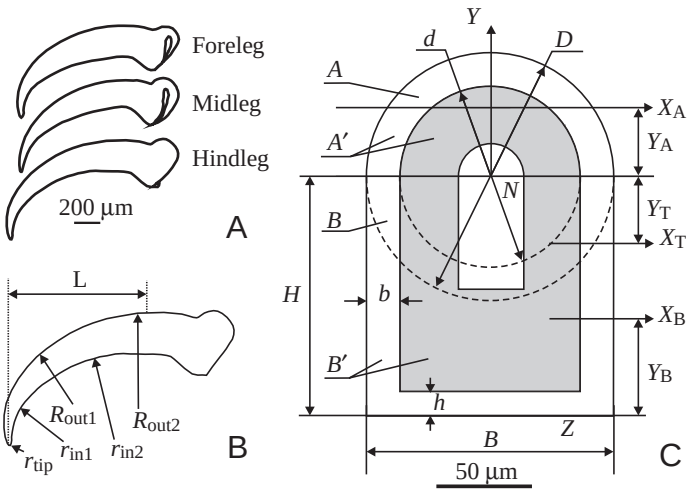

Fig. 2. Claw geometry. (A) Claw shape of the hind-, mid- and forelegs (drawings are based on SEM micrographs). (B) Five arcs used for quantitative description of the claw geometry (see Table 2). (C) Cross-section model of the claw for stress calculation. The model is based on SEM data (see Fig. 3E,F). The claw consists of three parts in its cross section: (1) a dense layer of the exocuticle (gray), (2) a loosely packed endocuticle, and the claw lumen. Semicircular (A′) and rectangular (B′) parts of the claw were calculated separately. X_A, X_B and X_T are bending centers of sections A, B and $A+B$, respectively. For an explanation of other symbols, see text, Table 3 and Appendix B.

medioposteriorly towards the body, whereas hindlegs push themselves posteriorly from the body (Fig. 2A–C). Typical claw lengths are 1.33, 1.20 and 1.21 mm for rear, middle and front claws, respectively. The claw shape of the fore-, mid- and hindlegs is very constant (Fig. 2A). The shape can be described as a set of five arcs (Fig. 2B, Table 2). At a high magnification the claw tip resembles a hemisphere (Fig. 3D).

The inner structure of a claw consists of three parts: (1) the outer, exocuticle part, 16.2±4.33 μm thick (N=2, n=11, where N is the number of individuals used and n is the number of claws measured), (2) the inner, endocuticle part, 26.2±3.5 μm thick (N=2, n=8) and (3) the central lumen (25.0–30.0 μm) (N=2, n=8) (Fig. 3E,F). The exocuticle is a very dense layer composed of thin lamella. The endocuticle consists of thicker lamellae, which seem to be not densely packed. Data on inner structure of lamellae (Fig. 3E) were used in the geometrical model of the claw (Fig. 2C).

Table 2. *Set of arcs describing the shape of claws in Pachnoda marginata in the fore-, mid- and hindlegs*

Radius (μm)	Forelegs	Midlegs	Hindlegs
Arc inside r_{in1}	269	421	336
Arc inside r_{in2}	1347	1235	752
Arc outside R_{out1}	402	457	397
Arc outside R_{out2}	938	925	918
Tip radius r	8.60	8.28	9.53

Arc notation is taken from Fig. 2B.

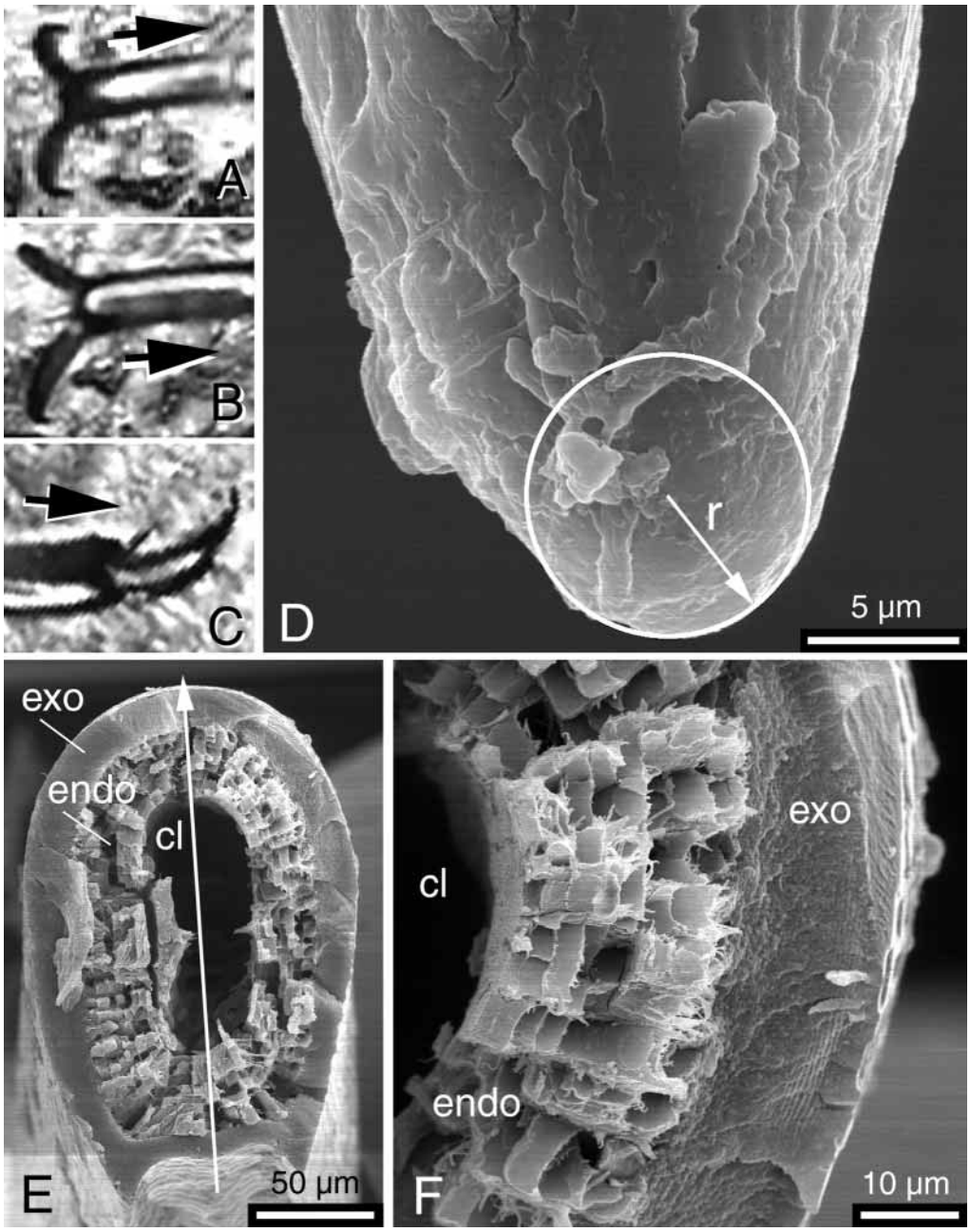

Fig. 3. Claws of *Pachnoda marginata*. (A–C) Claw positions of the foreleg (A), midleg (B) and hindleg (C) during walking on a rough surface. Black arrows indicate direction of leg movements. (D) SEM image of the claw tip. (E,F) SEM images of the claw fractured in the cross plane. The line of the arrow shows the symmetry axis of the claw and points to the dorsal direction. cl, claw lumen; endo, endocuticle; exo, exocuticle; r, radius of the tip hemisphere.

Breaking stress of the claw

Knowing the breaking force (Fig. 4B) and geometry of the claw (Fig. 2), the strength of the claw material can be calculated. During the break test, load linearly increased with the deflection distance, and suddenly decreased when the claw broke. Average breaking force was F_{bk}=197.6±7.7 mN at an average length of the bend beam L=0.38±0.04 mm (n=7). For further calculations, the claw was considered as a curved cantilever beam (Fig. 2). The mean bending torque $M=F_{bk}\cdot L$ was 7.51×10^{-5} N m. The maximum bending stress σ_{max} can be calculated by:

$$\sigma_{max} = \frac{M}{I_T} Y_T , \qquad (2)$$

where Y_T is the maximum distance from the flexural center X_T to the margin where tensile stress is maximal (Z in Fig. 2C). For the exocuticle part alone Y_T is 35.13 µm; for the exocuticle and endocuticle parts taken together, it is –2.177 µm. I_T is the moment of inertia for the bending-load bearing area. For the exocuticle part I_T is 10.01×10^6 µm^4; for the exocuticle and endocuticle parts taken together, it is 67.60×10^6 µm^4. The bending strength of the claw material was calculated to be 684.2–143.4 N mm^{-2}. For further calculation details, see Table 3 and Appendix B.

Claw lumen contains fluid that might influence the results of calculations, if it were in a closed volume; however, the lumen is connected to the body volume, so the water content of the lumen was not considered to be

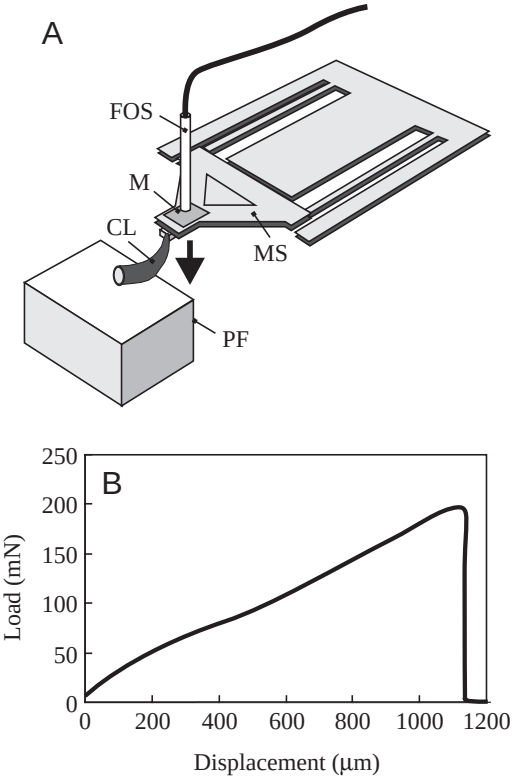

Fig. 4. Measurements of the mechanical strength of the claw. (A) Principle of force measurements using the force tester Basalt-01 (Tetra GmbH, Ilmenau, Germany). The claw (CL) was glued to the platform (PF). The metal spring (MS) was driven downwards by the piezo-drive until the claw was broken. Displacement of the spring tip equipped with a mirror M was detected in the vertical direction by the fiber optical sensor (FOS). (B) Force–distance curve obtained in experiments with the claw and used to calculate breaking stress of the claw.

an important factor influencing the breaking stress of the claw.

Friction force on different textures

The effect of surface roughness on the friction force of beetles was experimentally tested on a variety of sandpapers (Fig. 5A,B; Table 1). A typical force curve obtained in the experiments is shown in Fig. 5C. Maximum peaks and corresponding time were processed together with the beetle's position relative to the crossbeam (X). The force output by the beetle was calculated according to Equation 1.

Saturation of friction force was observed with increasing particle diameter of the substrate. Friction force rapidly increases with increased of particle diameter of the sandpaper in the range 12–50 μm (Fig. 5D). At particle diameters of 50–270 μm, only a very slight force increase was revealed. On rough textures, the forces were about 38 times higher than the average beetle weight. On relatively smooth textures the forces were comparable to the average weight of the beetle.

Table 3. *Calculation of the maximum bending stress of the claw*

Term	Equations	Exocuticle	Exocuticle+ endocuticle	Units
D		129.35		μm
d		94.55	39.47	μm
B		129.35		μm
b		17.38	44.92	μm
H		125.1		μm
h		12.39	39.93	μm
I_A	$I_A=0.00686(D^4-d^4)-\frac{0.0177D^2d^2(D-d)}{(D+d)}$	960667.09	1658113.70	μm^4
Y_A	$Y_A=\frac{2}{3\pi}\frac{D^2+Dd+d^2}{D+d}$	35.92	29.41	μm
I_B	$I_B=\frac{Bh^3+2b(H-h)^3}{12}+Bh\left(Y_B-\frac{h}{2}\right)^2+2b(H-h)\left(\frac{H-h}{2}+h-Y_B\right)^2$	8618001.24	59474144.34	μm^4
Y_B	$Y_B=\frac{Bh^2+2b(H^2-h^2)}{2[Bh+2b(H-h)]}$	50.586	114.62	μm
S_A	$S_A=\frac{\pi}{8}(D^2-d^2)$	3059.8	5958.64	μm^2
S_B	$S_B=2b(H-h)+Bh$	5520.45	12816.62	μm^2
I_T	$I_T=I_A+S_A(Y_A+Y_T)^2+I_B+S_B(H-Y_B-Y_T)^2$	10013484.52	67604619.72	μm^4
Critical	$\frac{\partial I_T}{\partial Y}=2S_A(Y_A+Y_T)+2S_B(H-Y_B-Y_T)(-1)=0$			
Y_T	$Y_T=\frac{S_B(H-Y_B)-S_AY_A}{S_A+S_B}$	35.13	–2.177	μm
Y_{max}	$Y_{max}=H-Y_T$	89.97	127.277	μm
σ_{max}	$\sigma_{max}=\frac{M}{I_{max}}Y_{max}$	684.2	143.4	N mm^{-2}

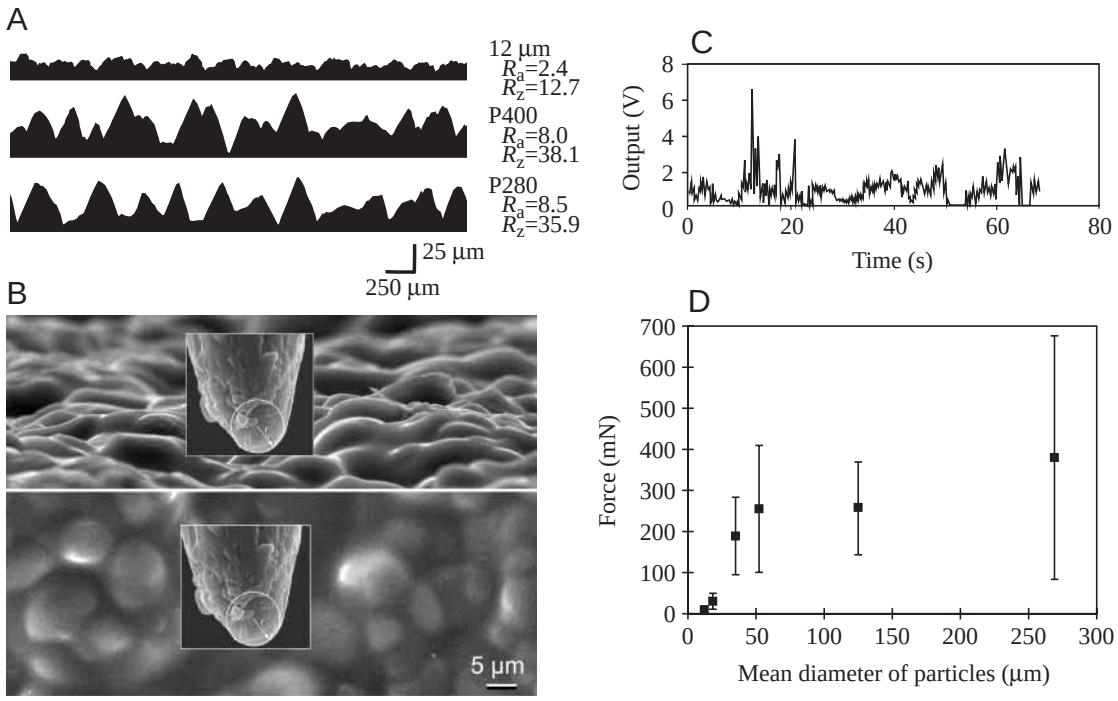

Fig. 5. Force generation by the beetle on different textures. (A) Surface texture of sandpaper types (12 µm, P400 and P280). R_a, surface roughness; R_z, average height of surface irregularities. (B) Comparison of the claw tip dimensions with the sandpaper texture (12 µm type) (above: side view, below: top view). (C) An example of the typical force recording used for data processing. (D) Forces generated by beetles walking on different substrate textures. When the diameter of particles is comparable with the claw tip, the claw slips out of the particle. When the diameter of the particles is larger than that of the claw tip, the claw is interlocked with the particles.

Output force of a single leg

Recordings were obtained separately for the fore- (n=62), mid- (n=45) and hindlegs (n=94). Only the maximum values from each recording were taken into account. Maximal force of a single leg ranged from 100 to 200 mN, which is about 10–20 times higher than the average weight of an animal (Fig. 6). However, during the test, 7.5 % of maximal values out of 94 hindleg recordings exceeded the upper measurement limit of the force sensor. Thus, the forces generated by hindlegs should be slightly higher than given in Fig. 6.

Comparison of force data obtained for single leg measurements with the data of the friction force at high particle diameters (Fig. 6) revealed that the average force output by six legs is higher than the friction force on very rough textures (Fig. 5D). The summarized force of six legs is about 550 mN, and a maximal value of the friction force is about 380 mN. The explanation of this fact is that beetles usually have 3–4 legs in the stance phase during walking. This means that the total force generated by the legs must be summarized not for 6 but for 3 legs.

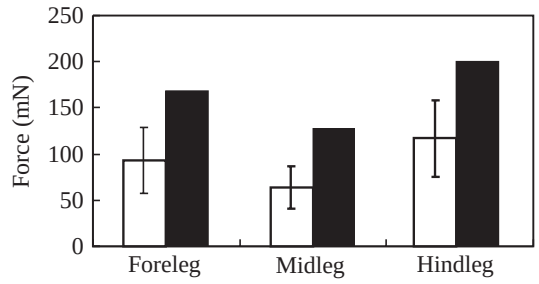

Fig. 6. Mean (white bars ± S.D.) and maximum (black bars) forces of the beetle legs (hindleg, n=94; midleg, n=45; foreleg, n=62).

Discussion

Tarsus control

In insects, claws are controlled by the action of a single muscle, the retractor unguis (Snodgrass, 1956; Gorb, 1996). Muscle contraction results in contact to the substrate during the stance phase of walking (Radnikow and Bässler, 1991). In the cockroach, previous kinematic and ablation studies demonstrated that, during walking, the multi-segmental structure of the tarsus, together with the elasticity of resilin-bearing elements of tarsal joints, aid in disengaging the contact of the claws with the substrate when the claw retractor muscle relaxes, and lift the tarsus together with the claws away from the substrate (Frazier et al., 1999). Such a design can facilitate the rapid and efficient use of the tarsus in walking while under active control by a single muscle. It may also be advantageous when an insect walks on a wavy substrate (Frazier et al., 1999).

Claw material

Breaking stress of the cuticle was previously measured in

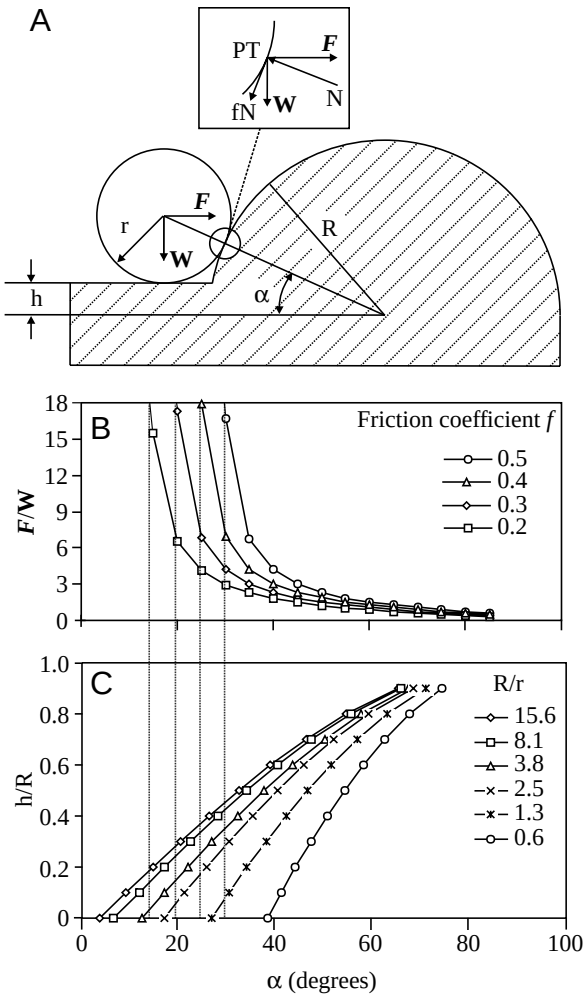

Fig. 7. Model of claw tip interaction with surface irregularities. (A) Geometry of the contact between the claw tip and a particle of the sandpaper. (B) Dependence of the force ratio ***F***/**W** on the contact angle (α) at different friction coefficients between the claw and particles of the sandpaper. (C) Dependence of h/R on the contact angle (α) at different values of the relationship $R_{PD}=R/r$ (particle radius/claw tip radius). When the diameter of a particle is comparable to the claw tip diameter ($R_{PD}=1$), both structures cannot interlock even at the friction coefficient $f=0.5$. When R_{PD} is greater than 4, the structures may interlock even at $f=0.2$. If the relationship between the immersion depth and particle radius (h/*R*) is >0.5, the relative maximum force ***F***/**W** is not larger than 5. The model predicts the relative maximum force depending on the friction coefficient at contact, the diameter of particles and the immersion depth. Broken lines divide ranges of α at which interlocking (self-locking) takes place (left side) at a particular friction coefficient; α, contact angle; ***F***, leg force; fN, line running perpendicular to the normal line N running through both centers of the particle and the claw tip; h, immersion depth of the hemispherical particle; r, claw radius; PT, contact point; R, particle radius; **W**, weight acting on the claw.

insect arthrodial membranes and solid cuticle of sclerites (Hepburn and Chandler, 1976). It is about five times higher in the solid (78.5±11.7 N mm^{-2}) than in the membranous cuticle (15.6 N mm^{-2}). In our experiment, breaking stress of the claw was evaluated to be 143.4 N mm^{-2}, if both exocuticle and endocuticle layers were taken into account. It is twofold higher than that of the solid cuticle of the locust. Presumably, a combination of the dense-layered exocuticle and loosely packed endocuticle plays a crucial role in the high strength of the claw material. The breaking stress of claw material is similar to that of vertebrate bones (88–174 N mm^{-2}) (Fung, 1993). Taking only the exocuticle part into account, the calculated breaking stress value (684.2 N mm^{-2}) was comparable to that of some types of steel (320–720 N mm^{-2}) (Pisarenko et al., 1988). In addition to the claw, high-strength properties can be expected in the cuticle of chewing and cutting mouthparts and in joint cuticle.

Model of the contact between claw tip and sandpaper particles

Friction force depends on the relationship between the dimensions of the claw tip and surface irregularities. When the surface roughness is lower than the radius of the claw tip, the claw slides over the substrate irregularities. Such a geometrical relationship results in low friction force. When the roughness is remarkably larger than the tip radius, claws tend to interlock with the substrate irregularities. Below we present a model which describes friction force of the claw on rough substrata.

According to the morphology of the claw, we can assume that the tip of the claw is part of a sphere (Figs 3D, 7A). Three assumptions were made about the substrate: (1) substrate irregularities are hemispherical; (2) all particles have the same diameter, corresponding to the mean diameter of the sandpaper particles; (3) each hemisphere is partly immersed in the glue at a depth of h (Fig. 7A). To reach a maximum force, the weight of the beetle has to be balanced by the horizontal force ***F***, assuming that the contact force between tip and glue surface is zero. An initial contact geometry of the model assumes two areas of claw contact: with the horizontal part of the substrate and with the particle. Two forces are acting on the claw tip: (1) the force generated by leg muscles and directed along the substrate surface (***F***); (2) animal weight, directed perpendicularly to the substrate surface (**W**). In this situation, the friction force will depend on the maximum frictional force when the claw slips on the particle surface. This is possible only when the angle α, describing the relationship between claw tip radius and particle size, is large enough. At a certain minimal α, sliding of the claw tip is prevented by the substrate particle, which results in the mechanical interlocking between the claw tip and the particle. In this case, the friction force entirely depends on the forces generated by the beetle.

The limiting situation is derived from the equilibrium condition. In the direction normal to the contact point, contact force **N**, based on the force equilibrium condition, is

$$\mathbf{N} = \boldsymbol{F}\cos\alpha + \mathbf{W}\sin\alpha\,. \quad (3)$$

In the tangent direction to the contacting point, we have

$$\boldsymbol{F}\sin\alpha = \mathbf{W}\cos\alpha + f\cdot\mathbf{N}\,, \quad (4)$$

where f is friction coefficient between claw tip and particle.

From equations 3 and 4, we have

$$\frac{\boldsymbol{F}}{\mathbf{W}} = \frac{\cos\alpha + f\sin\alpha}{\sin\alpha - f\cos\alpha} = \frac{1 + f\cdot\tan\alpha}{\tan\alpha - f}\,, \qquad (5)$$

where $\boldsymbol{F}/\mathbf{W}$ is the ratio of the force acting on the contact point in the horizontal direction to the force acting in the normal direction and f is the friction coefficient between the claw tip and particle. α (Fig. 7A) is defined as:

$$\sin\alpha = \frac{r + h}{r + R} = \frac{r/R + h/R}{r/R + 1}\,, \qquad (6)$$

where r=radius of claw tip. Thus from Equation 6, the deeper the immersion of particles in the glue (higher h), and/or the smaller the particle radius R, the greater the value of the angle α.

From Equation 5, the limit of the horizontal force $\boldsymbol{F}$ for a certain weight $\mathbf{W}$ can be obtained, when the angle α is big enough ($\tan\alpha - f > 0$). If the force generated by the beetle is greater than the limit, sliding will take place. In our experiment, such a situation was obtained at relatively low force (Fig. 5D). The force generated by the beetle on different surfaces can be predicted from Equation 5. For example, for sandpaper with particles of an average radius of 9.15 μm, the minimum contact angle is 28.81°, the predicted generated forces at h=0 are 46.18, 9.51, 3.38 and 2.46 mN for friction coefficients of 0.5, 0.4, 0.3 and 0.2, respectively. The predicted value at the friction coefficient of 0.5 corresponds well to the value of 30.4 mN measured in our experiments (Fig. 7B,C).

When particle radius is greater than that of the claw tip, Equation 5 results in a small contact angle α. This leads to a negative left part of equation 5 ($\tan\alpha - f < 0$), so that the claw interlocks itself with surface particles. The tip can remain stable and weight has no influence on the measured force. In this case, the measured force corresponds to the force generated by the beetle's leg muscles only. According to the model, a maximal horizontal force of 67.9 mN can be obtained on a surface with particles of an average radius of 26.1 μm at the friction coefficient 0.2, but this value is much lower than the value of 255 mN obtained in the experiment. The prediction seems to be reasonable, because the frictional coefficient of the beetle cuticle on the glass is about 0.35 (Z.D. and S.N.G., unpublished data). Claw interlocking (self-locking) takes place if the friction coefficient is not lower than 0.3. The h/R ratio has different limitations for various friction coefficients (h/R should be 0.04, 0.15 or 0.26 if the friction coefficients are 0.3, 0.4 or 0.5). The model explains why the force generated on surfaces with a particle diameter of 12–50 μm is low, and why it is high and varies slightly at a particle diameter of 50–270 μm.

Claw attachment system of insects and natural substrata

Insect attachment systems evolved as adaptations for efficient locomotion on a variety of surfaces. Insects usually walk on plant substrata, and, therefore, many aspects of insect–plant relationships deal with mechanical surface interactions. Presumably, such interactions are different in a variety of ecological groups of insects, such as herbivores and parasites, or specialist and generalist phytophages. From the plant perspective, completely different functions of the surface profile and coverage, such as insect trapping function and selective defense against herbivores, may involve similar general mechanisms.

Plant surfaces have a wide range of textures. They may be smooth, hairy or covered with waxes or moist secretions. The wax layer widely varies in thickness and has a crystalline structure. It is usually an extremely thin layer on the cuticles of aquatic plants, whereas substantial crusts appear as pruinescence on fruits, stems and leaves. The most common types of crystal shapes are tubes, solid rodlets, filaments, plates, ribbons and granules (Barthlott and Ehler, 1977; Barthlott and Wollenweber, 1981; Barthlott, 1998). Current classification of plant epicuticular waxes, based on high resolution scanning electron microscopy of 13,000 plant species, distinguishes 23 types of wax (Barthlott et al., 1998). Trichomes are hair-like protuberances extending from the epidermis of aerial plant tissues (Levin, 1973). They may be unicellular or multicellular, glandular or non-glandular, straight, spiral-shaped, hooked, unbranched or stellate. There are some examples of trichomes responsible for trapping insects and small animals in carnivorous plants, such as *Sarracenia purpurea*, *Genlisea* spp. and *Darlingtonia* spp. (Jeffree, 1986). Presumably, felted trichome layers provide a physical barrier against insect predators, protecting young leaves (Curtis and Lersten, 1978).

Adult *Pachnoda marginata* feed on diverse fruits and flowers but they can also burrow into the soil and walk on litter surface. That is why potential surface roughness in nature remains unpredictable for this species. Our work shows that surface roughness strongly influences the attachment abilities of the insect claw system. Insect tarsi equipped only with claws can attach to a vertical surface only at a substrate roughness comparable to or bigger than the diameter of the claw tips. Thus, it can be concluded that by the mediation of the surface roughness, plants may change insect–plant interaction. Our work is a step towards understanding which type of attachment device is optimized for a plant surface with particular properties. The scaling effects and the role of mechanical properties of substrate material, however, remain poorly understood. Further comparative studies on the texture of plant surfaces and dimensions of insect claw tips may complete the proposed model.

Appendix A

Calculation of the surface roughness

The R_a is defined as the square root value of the surface profile:

$$R_a = \sqrt{\frac{1}{n}\sum_{j=1}^{n}[s(x) - \bar{s}(x)]^2}\,, \qquad (A1)$$

where $s(x)$ is the surface height at point x in surface profile, $\bar{s}(x)$ is the average height of the surface profile, and n is the number of points.

Appendix B

Calculation of the bending stress of the claw

Presumably, the exocuticle and endocuticle layers have different material properties. Since the differences are not known, the breaking stress of the claw was calculated in two ways. In the first one, only the geometry of the exocuticle layer was taken into account. In this case, calculated stress is higher than the real stress. In the second one, both layers (exocuticle and endocuticle) were taken into account, assuming that both of them have the same material properties. In this case, calculated stress is lower than the real stress. The real stress probably has an intermediate value somewhere between the results of these approaches.

The moment of inertia I_A for part A of the claw is

$$I_A = 0.00686(D^4 - d^4) - \frac{0.0177D^2d^2(D-d)}{(D+d)}, \quad \text{(B1)}$$

where D and d are the diameters of the outer and inner circles of the cross section of the claw.

The distance Y_A from the flexural center X_A of part A to its boundary N (Fig. 1) is:

$$Y_A = \frac{2}{3\pi}\,\frac{D^2 + Dd + d^2}{D+d}. \quad \text{(B2)}$$

The moment of inertia I_B for part B of the claw is:

$$I_B = \frac{Bh^3 + 2b(H-h)^3}{12} + Bh\left(Y_B - \frac{h}{2}\right)^2 + 2b(H-h)\left(\frac{H-h}{2} + h - Y_B\right)^2, \quad \text{(B3)}$$

where B and b are widths of the bending squares (Fig. 2C) and H and h are the heights of bending squares.

The distance Y_B from the flexural center X_B of part B to its boundary Z (Fig. 2) is:

$$Y_B = \frac{Bh^2 + 2b(H^2 - h^2)}{2[Bh + 2b(H-h)]}. \quad \text{(B4)}$$

The two parts taken together give the total bending modulus I_T:

$$I_T = I_A + S_A(Y_A + Y)^2 + I_B + S_B(H - Y_B - Y)^2, \quad \text{(B5)}$$

where S_A and S_B are areas of sections A and B:

$$S_A = \frac{\pi}{8}(D^2 - d^2), \quad \text{(B6)}$$

and

$$S_B = 2b(H-h) + Bh. \quad \text{(B7)}$$

Y_T is the distance from the flexural center X_T of the whole structure to the boundary N (Fig. 2). It is determined as:

$$\frac{\partial I_T}{\partial Y}\,2S_A(Y_A + Y_T) + 2S_B(H - Y_B - Y_T)(-1) = 0, \quad \text{(B8)}$$

$$Y_T = \frac{S_B(H - Y_B) - S_A Y_A}{S_A + S_B} \quad \text{(B9)}$$

and

$$I_T = I_A + S_A(Y_A + Y_T)^2 + I_B + S_B(H - Y_B - Y_T)^2. \quad \text{(B10)}$$

The distance from the flexural center to the point with maximum tensile bending stress is $Y_{max}=H–Y$. The bending stress can be then obtained from

$$\sigma_{max} = \frac{M}{I_T}\,Y_{max}. \quad \text{(B11)}$$

List of symbols

B, b	Widths of the bending squares
D	Height of crossbeam from sandpaper surface
D, d	Diameters of the outer and inner circles, respectively, of the cross section of the claw
f	Friction coefficient between the claw tip and particle
F_{bk}	Average breaking force of claw
$\boldsymbol{F}$	Force generated by leg muscles and directed along the surface
F_S	Force monitored by the sensor
F_B	Force generated by the beetle
H, h	Heights of bending squares
h	Immersion depth of particles in the glue
I_A	Moment of inertia for part A of the claw
I_B	Moment of inertia for part B of the claw
I_T	Moment of inertia for the bending-load bearing area A and B
L	Average length of the bend beam of the claw
M	Mean bending torque acting on the claw
N	Boundary running through centre of outer and inner circles
N	Normal force between the claw and particle
r	Radius of the claw tip
R	Particle radius
R_a	Surface roughness
R_z	average height of surface irregularities
S_A, S_B	Areas of sections of parts A and B, respectively
X	Distance from beetle to sensor beam
X	Distance between the sensor to the contact point of the Plexiglas angle on the crossbeam
X_T	Flexural centre
Y_A	Distance from the flexural center X_A of part A to its boundary N
Y_B	Distance from the flexural center X_B of part B to its boundary Z
Y_T	Maximum distance from the flexural center X_T to the boundary N

Y_{max}	Distance from X_T to point of σ_{max}
W	Weight acting on the claw
Z	Boundary of flat part of the claw section
$s(x)$	Surface height at point x in the surface profile
$\bar{s}(x)$	Average height of the surface profile
n	Number of points measured for the surface profile
α	Contact angle
σ_{max}	Maximum bending stress of the claw

Sincere thanks to J. Berger for help with SEM preparations, W. Vötsch for help with video equipment and V. Kastner for linguistic corrections. Two anonymous reviewers provided valuable suggestions and points for discussion. This work was supported by the Federal Ministry of Science of Germany (BMBF) grant BioFuture 0311851 to S.G.

References

Barthlott, W. (1998). Scanning electron microscopy of the epidermal surface in plants. In *Scanning Electron Microscopy in Taxonomy and Functional Morphology* (ed. D. Claugher), pp. 69–94. Oxford: Clarendon Press.

Barthlott, W. and Ehler, N. (1977). Raster-Elektronenmikroskopie der Epidermisoberflächen von Spermatophyten. *Trop. Subtrop. Pflanzenwelt* **19**, 367–467.

Barthlott, W., Neinhuis, C., Cutler, D., Ditsch, F., Meusel, I., Theisen, I. and Wilhelmi, H. (1998). Classification and terminology of plant epicuticular waxes. *Bot. J. Linn. Soc.* **126**, 237–260.

Barthlott, W. and Wollenweber, E. (1981). Zur Feinstruktur, Chemie und taxonomischen Signifikanz epikutikularer Wachse und ähnliche Sekrete. *Trop. Subtrop. Pflanzenwelt* **32**, 7–67.

Bauchhenss, E. (1979). Die Pulvillen von *Calliphora erythrocephala* Meig. (Diptera, Brachycera) als Adhäsionsorgane. *Zoomorphologie* **93**, 99–123.

Cartmill, M. (1985). Climbing. In *Functional Vertebrate Morphology* (ed. M. Hildebrand, D. M. Bramble, K. F. Liem and D. B. Wake), pp. 73–88. Cambridge: The Belknap Press.

Curtis, J. D. and Lersten, N. R. (1978). Heterophylly in *Populus grandidentala* (Salicaceae) with emphasis on resin glands and extrafloral nectaries. *Am. J. Bot.* **65**, 1003–1010.

Eisner, T. and Aneshansley, D. J. (2000). Defence by foot adhesion in a beetle (*Hemisphaerota cyanea*). *Proc. Natl. Acad. Sci. USA* **97**, 6568–6573.

Federle, W., Brainerd, E. L., McMahon, T. A. and Hölldobler, B. (2001). Biomechanics of the movable pretarsal adhesive organ in ants and bees. *Proc. Natl. Acad. Sci. USA* **98**, 6215–6220.

Federle, W., Rohrseitz, K. and Hölldobler, B. (2000). Attachment forces of ants measured with a centrifuge: better 'wax-runners' have a poorer attachment to a smooth surface. *J. Exp. Biol.* **203**, 505–512.

Frazier, S. F., Larsen, G. S., Neff, D., Quimby, L., Carney, M., DiCaprio, R. A. and Zill, S. N. (1999). Elasticity and movements of the cockroach tarsus in walking. *J. Comp. Physiol. A* **185**, 157–172.

Fung, Y. C. (1993). *Biomechanics: Mechanical properties of living tissues*. Second edition. Berlin: Springer.

Gillett, J. D. and Wigglesworth, V. B. (1932). The climbing organ of an insect, *Rhodnius prolixus* (Hemiptera, Reduviidae). *Proc. R. Soc. Lond. B* **111**, 364–376.

Gorb, S. N. (1996). Design of insect unguitractor apparatus. *J. Morphol.* **230**, 219–230.

Gorb, S. N. (1998). The design of the fly adhesive pad: distal tenent setae are adapted to the delivery of an adhesive secretion. *Proc. R. Soc. Lond. B* **265**, 747–752.

Gorb, S. N., Jiao, Y. and Scherge, M. (2000). Ultrastructural architecture and mechanical properties of attachment pads in *Tettigonia viridissima* (Orthoptera Tettigoniidae). *J. Comp. Physiol. A* **186**, 821–831.

Heinzeller, J., Seifert, P. and Aschauer, B. (1989). Architektur des Unguitraktor-Apparatus bei *Chironomus thummi* (Diptera). *Verh. Dtsch. Zool. Ges.* **82**, 260.

Hepburn, H. R. and Chandler, H. D. (1976). Material properties of arthropod cuticles: the arthrodial membranes. *J. Comp. Physiol. A* **109**, 177–198.

Ishii, S. (1987). Adhesion of a leaf feeding ladybird *Epilachna vigintioctomaculata* (Coleoptera: Coccinellidae) on a vertically smooth surface. *Appl. Ent. Zool.* **22**, 222–228.

Jeffree, C. E. (1986). The cuticle, epicuticular waxes and trichomes of plants, with references to their structure, functions and evolution. In *Insects and the Plant Surface* (ed. B. E. Juniper and T. R. E. Southwood), pp. 23–64. London: Edward Arnold.

Jiao, Y., Gorb, S. N. and Scherge, M. (2000). Adhesion measured on the attachment pads of *Tettigonia viridissima* (Orthoptera, Insecta). *J. Exp. Biol.* **203**, 1887–1895.

Levin, D. A. (1973). The role of trichomes in plant defence. *Q. Rev. Biol.* **48**, 3–15.

Nachtigall, W. (1974). *Biological Mechanisms of Attachment.* Berlin, Heidelberg, New York: Springer-Verlag.

Pisarenko, G. S., Yakovlev, A. P. and Matveev, V. V. (1988). *Handbook on Material Mechanics*. Kiev: Naukova Dumka (in Russian).

Radnikow, G. and Bässler, U. (1991). Function of a muscle whose apodeme travels through a joint moved by other muscles: why the retractor unguis muscle in stick insects is tripartite and has no antagonist. *J. Exp. Biol.* **157**, 87–99.

Seifert, P. and Heinzeller, T. (1989). Mechanical, sensory and glandular structures in the tarsal unguitractor apparatus of *Chironomus riparius* (Diptera, Chironomidae). *Zoomorphol.* **109**, 71–78.

Snodgrass, R. E. (1956). *Anatomy of the Honey Bee*. New York: Comstock Publishing Associates.

Stork, N. E. (1980). Experimental analysis of adhesion of *Chrysolina polita* (Chrysomelidae, Coleoptera) on a variety of surfaces. *J. Exp. Biol.* **88**, 91–107.

Stork, N. E. (1983a). A comparison of the adhesive setae on the feet of lizards and arthropods. *J. Nat. Hist.* **17**, 829–835.

Stork, N. E. (1983b). The adherence of beetle tarsal setae to glass. *J. Nat. Hist.* **17**, 583–597.

Stork, N. E. (1987). Adaptations of arboreal carabids to life in trees. *Acta Phytopathol. Entom. Hungarica* **22**, 273–291.

Walker, G., Yule, A. B. and Ratcliffe, J. (1985). The adhesive organ of the blowfly, *Calliphora vomitoria*: a functional approach (Diptera: Calliphoridae). *J. Zool. Lond.* **205**, 297–307.